

# q-Analogue of Hamiltonian Monte Carlo method

Xiaomei Yang

School of Mathematics

Southwest Jiaotong University

yangxiaomath@swjtu.edu.cn

Zhiliang Deng

School of Mathematical Sciences

University of Electronic Science and Technology of China

dengzhl@uestc.edu.cn

December 16, 2025

## Abstract

Building upon Lagrangian mechanics on Wess's  $q$ -commutative spaces, we derive the  $q$ -deformed Hamiltonian dynamics as formulated by Lavagno et al. (2006). We then develop a computationally tractable scheme and propose a novel Hamiltonian Monte Carlo sampler ( $q$ -HMC). The proposed  $q$ -HMC method is shown to satisfy the detailed balance principle. Numerical experiments on distributions with explicit potential functions demonstrate its efficacy, particularly in exploring stiff energy landscapes. This method is also applied to draw samples from the Bayesian posterior distribution of inverse problems. The numerical test for the posterior distribution with stiff potential further shows the advantage of  $q$ -HMC. And it yields the identical computational implementation process to that of HMC when used to deal with functional reconstruction problems.

## 1 Introduction

The core challenge in statistical computing is to extract information from a probability distribution

$$\pi(x) \propto \exp(-U(x)), \quad (1)$$

where  $U(x)$  is the potential function. A prominent method for sampling from such distributions is Hamiltonian Monte Carlo (HMC) [2–4, 6, 7, 18, 19, 21, 22]. HMC explores the parameter space by simulating Hamiltonian dynamics in an augmented phase space to generate efficient, long-range proposals. A suitable numerical integrator yields high sampling efficiency due to the symplectic structure of the Hamiltonian system. However, when the Hamiltonian ordinary differential equations (ODEs) are stiff, the numerical integrator must be chosen with care [13]. The standard Leap-Frog scheme, for instance,

often imposes severe time step restrictions for stability due to its sensitivity to such stiffness. To achieve novel sampling behaviors and enhanced robustness, an alternative way is to explore replacements for the Hamiltonian system itself.

In this paper, we investigate a  $q$ -analogue of HMC ( $q$ -HMC) for sampling from target distributions. The methodology draws inspiration from  $q$ -deformed quantum mechanics, where the algebra is defined by generators and their  $q$ -commutation relations [1, 5, 11, 12, 25]. Within this algebra, the fundamental deformation parameter  $q$  bridges the classical commutative case at  $q = 1$  with a broad spectrum of noncommutative structures for  $q \neq 1$ . This offers a natural generalization of the canonical formalisms in classical and quantum mechanics, and a more versatile mathematical structure for modeling complex physical systems. The utility of such deformations has been demonstrated in various applications, including studies of the hydrogen atom [10, 14, 23] and the quantum harmonic oscillator through  $q$ -deformed Schrödinger equations [8, 9, 15, 16, 20, 26, 27].

In [17], a  $q$ -deformed Hamiltonian system are established via non-commutative  $q$ -calculus. We here derive the same  $q$ -deformed Hamiltonian dynamics in the framework of the Lagrangian mechanics. This system is transferred into the computationally tractable one. We then present the  $q$ -HMC from the computation scheme and show that it satisfies the detailed balance principle. This approach can be effectively applied to sample from various target distributions. It is of advantage when dealing with distributions with stiff potential functions. And when applied to some Bayesian inverse problems, its computational procedure is proved to be identical to that of classical HMC for some functional reconstruction problems.

The rest of the paper proceeds as follows. Building on the principles of Lagrangian mechanics, Section 2 derives the formulation of the  $q$ -deformed Hamiltonian system in [17]. Then based on the  $q$ -deformation, a numerically tractable  $q$ -analogue of Hamiltonian dynamics is presented. The  $q$ -HMC algorithm is established in Section 3. Section 4 provides numerical tests to evaluate the method's performance across distributions with different potential functions. And an application to Bayesian inverse problems is detailed in Section 5. Final conclusions are drawn in Section 6.

## 2 $q$ -analogue Hamiltonian dynamics

In this section, we introduce the preliminary concepts of  $q$ -calculus and employ them to derive the  $q$ -deformed Hamiltonian system from the principles of Lagrangian mechanics. The  $q$ -deformed Hamiltonian system is first introduced in [17] via the  $q$ -Poisson bracket. For this system, we present a numerically tractable scheme, which is also a  $q$ -analogue of Hamiltonian dynamics.

Let the operators  $\hat{x}$  and  $\hat{p}$  satisfy the  $q$ -commutation relation

$$\hat{p}\hat{x} = q\hat{x}\hat{p}, \quad (2)$$

with  $q$  being a real deformation parameter. This relation is invariant under the action of the quantum group  $\text{GL}_q(2)$ . The real quantum plane  $\hat{\mathbb{R}}^2$  is defined as the space generated by the basis elements  $e_x \equiv \hat{x}$  and  $e_p \equiv \hat{p}$ . We denote by  $\hat{\mathcal{A}} = \text{Fun}(\hat{\mathbb{R}}^2)$  the associative algebra freely generated by the elements  $\hat{x}$  and  $\hat{p}$ . The  $q$ -tangent space  $T\hat{\mathcal{A}}$  is generated

by the  $q$ -derivatives  $\tilde{\partial}_x \equiv \hat{\partial}_{\hat{x}}$  and  $\tilde{\partial}_p \equiv \hat{\partial}_{\hat{p}}$  whose action on the generators is defined as

$$\tilde{\partial}_x e_x = 1, \quad \tilde{\partial}_x e_p = 0, \quad \tilde{\partial}_p e_x = 0, \quad \tilde{\partial}_p e_p = 1. \quad (3)$$

The relations between variables and derivatives have shown to be [24]

$$\begin{aligned} \hat{\partial}_{\hat{p}} \hat{x} &= q \hat{x} \hat{\partial}_{\hat{p}}, \\ \hat{\partial}_{\hat{x}} \hat{p} &= q \hat{p} \hat{\partial}_{\hat{x}}, \\ \hat{\partial}_{\hat{p}} \hat{p} &= 1 + q^2 \hat{p} \hat{\partial}_{\hat{p}} + (q^2 - 1) \hat{x} \hat{\partial}_{\hat{x}}, \\ \hat{\partial}_{\hat{x}} \hat{x} &= 1 + q^2 \hat{x} \hat{\partial}_{\hat{x}}, \\ \hat{\partial}_{\hat{p}} \hat{\partial}_{\hat{x}} &= q^{-1} \hat{\partial}_{\hat{x}} \hat{\partial}_{\hat{p}}. \end{aligned} \quad (4)$$

Let  $\hat{v} := \dot{\hat{x}}$  denote the  $q$ -deformed velocity. The Lagrangian is denoted by  $\hat{\mathcal{L}} = \hat{\mathcal{L}}(\hat{x}, \hat{v})$ . The corresponding  $q$ -deformed momentum  $\hat{p}$  is defined as the left action of the velocity derivative on the Lagrangian:

$$\hat{p} = q^{1/2} \left( \hat{\partial}_{\hat{v}} \hat{\mathcal{L}} \right)^L, \quad (5)$$

which is still subject to the  $q$ -commutative relationship (2). Here, the superscript  $L$  denotes that the operator acts from the left, and the superscript  $R$  would signify a right action on a function. The  $q$ -deformed Euler–Lagrange equation is then given by

$$\frac{d}{dt} \left( \hat{\partial}_{\hat{v}} \hat{\mathcal{L}} \right)^L - \left( \hat{\partial}_{\hat{x}} \hat{\mathcal{L}} \right)^L = 0, \quad (6)$$

which follows from the stationary value of the action integral

$$S = \int \hat{\mathcal{L}}(\hat{x}, \hat{v}) dt.$$

The  $q$ -deformed Euler–Lagrange equation (6) together with (5) yields that

$$\dot{\hat{p}} = q^{1/2} \left( \hat{\partial}_{\hat{x}} \hat{\mathcal{L}} \right)^L.$$

The differential of the Lagrangian  $\hat{\mathcal{L}}$  is

$$\begin{aligned} d\hat{\mathcal{L}} &= d\hat{x} \left( \hat{\partial}_{\hat{x}} \hat{\mathcal{L}} \right)^L + d\hat{v} \left( \hat{\partial}_{\hat{v}} \hat{\mathcal{L}} \right)^L \\ &= q^{-1/2} (d\hat{x} \cdot \dot{\hat{p}} + d\hat{v} \cdot \hat{p}) \\ &= q^{-1/2} (d\hat{x} \cdot \dot{\hat{p}} + d(\hat{v} \cdot \hat{p}) - \hat{v} \cdot d\hat{p}). \end{aligned} \quad (7)$$

The  $q$ -deformed Hamiltonian is defined via the Legendre transform of  $\hat{\mathcal{L}}$ :

$$\hat{H}(\hat{x}, \hat{p}) := q^{-1/2} \hat{v} \cdot \hat{p} - \hat{\mathcal{L}}(\hat{x}, \hat{v}).$$

And the corresponding  $q$ -Hamilton's equations are given by (7)

$$d\hat{H} \equiv d \left( q^{-1/2} \hat{v} \cdot \hat{p} - \hat{\mathcal{L}} \right) = q^{-1/2} (\hat{v} \cdot d\hat{p} - d\hat{x} \cdot \dot{\hat{p}}).$$

We hence get the  $q$ -deformed Hamiltonian equations from  $d\hat{H} = d\hat{x} \left( \hat{\partial}_{\hat{x}} \hat{H} \right)^L + d\hat{p} \left( \hat{\partial}_{\hat{p}} \hat{H} \right)^L$

$$\begin{aligned}\dot{\hat{x}} &= q^{-1/2} \left( \hat{\partial}_{\hat{p}} \hat{H} \right)^L, \\ \dot{\hat{p}} &= -q^{1/2} \left( \hat{\partial}_{\hat{x}} \hat{H} \right)^L.\end{aligned}\tag{8}$$

These equations are consistent with those in [17] and reduce to the classical Hamiltonian system as  $q \rightarrow 1$ .

Next, we transfer (8) into a numerically tractable scheme by the replacements [17, 24]

$$\hat{x} \rightarrow x, \hat{p} \rightarrow pD_x, \hat{\partial}_{\hat{x}} \rightarrow \mathcal{D}_x, \hat{\partial}_{\hat{p}} \rightarrow \mathcal{D}_p D_x, \tag{9}$$

where  $D_x f(x, p) = f(qx, p)$  is the dilatation operator along the  $x$  direction,  $\mathcal{D}_x, \mathcal{D}_p$  are the Jackson derivatives with respect to  $x$  and  $p$  defined by

$$\begin{aligned}\mathcal{D}_x f(x, p) &= \frac{f(q^2 x, p) - f(x, p)}{(q^2 - 1)x}, \\ \mathcal{D}_p f(x, p) &= \frac{f(x, q^2 p) - f(x, p)}{(q^2 - 1)p}.\end{aligned}\tag{10}$$

By some computations and simplifications, the scheme is given as follows

$$\begin{aligned}\dot{x} &= q^{-1/2} \mathcal{D}_p [H(qx, p)], \\ \dot{p} &= -q^{1/2} \mathcal{D}_x [H(x, p)],\end{aligned}\tag{11}$$

where  $x, p$  and  $H$  denote the classical variables and Hamiltonian function. Define the  $q$ -analogue of Poisson bracket by

$$\{f, g\}_q = q^{-1/2} \mathcal{D}_p D_x g \cdot \mathcal{D}_x f - q^{1/2} \mathcal{D}_x g \cdot \mathcal{D}_p f. \tag{12}$$

The  $q$ -analogue (11) can be then written as

$$\begin{aligned}\dot{x} &= \{x, H\}_q, \\ \dot{p} &= \{p, H\}_q.\end{aligned}\tag{13}$$

Equations (11) (or (13)) are also viewed as a generalization of the Hamiltonian system since it reduces to the classical case as  $q \rightarrow 1$ . We call (11) (or (13)) the  $q$ -analogue of Hamiltonian dynamics or  $q$ -Hamiltonian system. Because the  $q$ -Hamiltonian system is more computationally tractable than the system in (8), it is suited for simulation.

### 3 $q$ -Hamiltonian Monte Carlo

In this section, we explore the use of  $q$ -Hamiltonian system to sample from the distribution (1). We assume that the target probability density  $\pi(x)$  is defined on  $\mathbb{R}^d$  with respect to the Lebesgue measure.

We define the augmented phase space  $\mathbb{R}^d \times \mathbb{R}^d$ , where  $x \in \mathbb{R}^d$  represents the position variable (corresponding to the parameters of interest), and  $p \in \mathbb{R}^d$  is the momentum variable. In the phase space, let  $z := (x, p)$  admit the distribution

$$\pi(z) = \pi(x, p) \propto \exp(-H(x, p)). \tag{14}$$

where  $H$  is the Hamiltonian representing the total energy of the system. Assume that  $x$ ,  $p$  evolve with the  $q$ -Hamiltonian equations (11) or (13) and  $H(x, p)$  is of this form

$$H(x, p) = U(x) + K(x, p). \quad (15)$$

Following the classical HMC approach, we discretize the  $q$ -Hamiltonian equation (11) with the Leap-Frog scheme

$$\begin{aligned} p^{n+1/2} &= p^n - \frac{\Delta t}{2} F(x^n, p^n) := \mathbf{A}_{\frac{\Delta t}{2}}(x^n, p^n), \\ x^{n+1} &= x^n + \Delta t v(x^n, p^{n+1/2}) := \mathbf{B}_{\Delta t}(x^n, p^{n+1/2}), \\ p^{n+1} &= p^{n+1/2} - \frac{\Delta t}{2} F(x^{n+1}, p^{n+1/2}) = \mathbf{A}_{\frac{\Delta t}{2}}(x^{n+1}, p^{n+1/2}), \end{aligned} \quad (16)$$

where

$$\begin{aligned} v &= q^{-1/2} \mathcal{D}_p[H(qx, p)], \\ F &= q^{1/2} \mathcal{D}_x[H(x, p)]. \end{aligned} \quad (17)$$

The Leap-Frog integrator can be represented by the operator

$$\phi_{\Delta t} = \mathbf{A}_{\frac{\Delta t}{2}} \circ \mathbf{B}_{\Delta t} \circ \mathbf{A}_{\frac{\Delta t}{2}}, \quad (18)$$

Based on the  $q$ -Hamiltonian system (11) and the Leap-Frog scheme (16), we propose a  $q$ -HMC sampling algorithm as follows:

---

**Algorithm 1**  $q$ -HMC

---

**Require:** Target distribution  $\pi(x) \propto \exp(-U(x))$ , current state  $x_{\text{curr}}$ , step size  $\Delta t$ , number of steps  $L$ , parameter  $q$ .

**Ensure:** Next sample  $x_{\text{next}}$ .

**1: Initialization:**

Sample momentum  $p \sim \pi_K(p|x_{\text{curr}}) \propto \exp(-K(x_{\text{curr}}, p))$ .  
 Compute initial Hamiltonian  $H_{\text{init}} = H(x_{\text{curr}}, p)$ .  
 Initialize  $q$ -Jacobian determinant:  $J \leftarrow 1.0$ .

**2: Proposal Generation**

$(x^*, p^*, J) \leftarrow \text{LeapFrog}(x_{\text{curr}}, p, q, \Delta t, L, J)$ .  
 Compute final Hamiltonian  $H_{\text{final}} = H(x^*, p^*)$ .

**3: Metropolis Accept/Reject:**

Compute the acceptance probability  $\alpha$ :

$$\alpha = \min(1, J \cdot \exp(H_{\text{init}} - H_{\text{final}})).$$

Draw uniform random number  $u \sim \mathcal{U}(0, 1)$ .

If  $u < \alpha$ ,  $x_{\text{next}} \leftarrow x^*$ ; else,  $x_{\text{next}} \leftarrow x_{\text{curr}}$ .

**4: Return**  $x_{\text{next}}$ .

---

To simplify the discussions, we consider 1-dimensional case, i.e.,  $d = 1$ . Let  $\mathbf{T}$  denote the time reversible operator, i.e.,  $\mathbf{T}(x, p) = (x, -p)$ . By  $\left(\frac{\partial \mathbf{S}}{\partial z}\right)_q$ , we denote the  $q$ -Jacobian matrix of  $\mathbf{S} = (\mathbf{S}_1(x, p), \mathbf{S}_2(x, p))$  w.r.t.  $z$ , i.e.,

$$\left(\frac{\partial \mathbf{S}}{\partial z}\right)_q = \begin{bmatrix} \mathcal{D}_x \mathbf{S}_1 & \mathcal{D}_p \mathbf{S}_1 \\ \mathcal{D}_x \mathbf{S}_2 & \mathcal{D}_p \mathbf{S}_2 \end{bmatrix}.$$

Assume that the kinetic energy  $K$  satisfies

$$K(x, -p) = K(x, p). \quad (19)$$

The momentum sampling step in Algorithm 1 satisfies the detailed balance relation, i.e.,

$$\pi(x, p)\pi_K(p_{new}|x) = \pi(x, p_{new})\pi_K(p|x).$$

We subsequently consider the detailed balance relation of the transition step. The transition probability is given by

$$\begin{aligned} P(z \rightarrow z') = & \kappa(z \rightarrow z^*)\alpha(z \rightarrow z^*)\delta(z' - z^*) \\ & + \left[ \delta(z' - z) \int \kappa(z \rightarrow z^*)(1 - \alpha(z \rightarrow z^*))dz^* \right], \end{aligned} \quad (20)$$

where  $\kappa(z \rightarrow z^*) = \delta(z^* - \Psi(z))$  and  $\Psi(z) = \mathbf{T} \circ \phi_{L\Delta t}(z)$ .

**Proposition 1.** *Assume that the kinetic energy function  $K$  satisfies (19). Then the Leap-Frog scheme is time reversibility, i.e.,  $\mathbf{T} \circ \phi_{\Delta t} \circ \mathbf{T} = \phi_{-\Delta t} = \phi_{\Delta t}^{-1}$ .*

*Proof.* The momentum update  $\mathbf{A}_{\Delta t} : (x, p) \rightarrow (x, p - \Delta t F(x, p))$ . Since  $F(x, -p) = F(x, p)$ , we can get

$$\mathbf{T} \circ \mathbf{A}_{\Delta t} \circ \mathbf{T} = \mathbf{A}_{-\Delta t}.$$

In addition, since the velocity function  $v$  satisfies  $v(x, -p) = -v(x, p)$ , we have

$$\mathbf{T} \circ \mathbf{B}_{\Delta t} \mathbf{T} = \mathbf{B}_{-\Delta t}.$$

Therefore, we get  $\mathbf{T} \circ \phi_{\Delta t} \circ \mathbf{T} = \phi_{-\Delta t}$  by  $\mathbf{T} \circ \mathbf{T} = I$ . It is easy to verify

$$\begin{aligned} \mathbf{A}_{\Delta t}^{-1} &= \mathbf{A}_{-\Delta t}, \\ \mathbf{B}_{\Delta t}^{-1} &= \mathbf{B}_{-\Delta t}. \end{aligned}$$

Therefore we have

$$\phi_{\Delta t}^{-1} = \phi_{-\Delta t}.$$

□

**Proposition 2.** *Let Hamiltonian be defined by (15). For Leap-Frog integrator (18), the  $q$ -Jacobian determinant*

$$J_{\Delta t} = \det \left( \frac{\partial \mathbf{A}_{\frac{\Delta t}{2}}}{\partial z_0} \right)_q \cdot \det \left( \frac{\partial \mathbf{B}_{\Delta t}}{\partial z_{1/2}} \right)_q \cdot \det \left( \frac{\partial \mathbf{A}_{\frac{\Delta t}{2}}}{\partial z_1} \right)_q, \quad (21)$$

where  $z_0$  is the initial state,  $z_{1/2} = \mathbf{A}_{\frac{\Delta t}{2}}(z_0)$ ,  $z_1 = \mathbf{B}_{\Delta t}(z_{1/2})$  and

$$\begin{aligned} \det \left( \frac{\partial \mathbf{A}_{\frac{\Delta t}{2}}}{\partial z_0} \right)_q &= 1 + \frac{\Delta t}{2} \mathcal{D}_p F(z_0), \\ \det \left( \frac{\partial \mathbf{B}_{\Delta t}}{\partial z_{1/2}} \right)_q &= 1 + \Delta t \mathcal{D}_x v(z_{1/2}), \\ \det \left( \frac{\partial \mathbf{A}_{\frac{\Delta t}{2}}}{\partial z_1} \right)_q &= 1 + \frac{\Delta t}{2} \mathcal{D}_p F(z_1). \end{aligned}$$

*Proof.* The computation is direct and we omit it here.  $\square$

**Theorem 3.1.** *Let the kinetic energy  $K$  satisfy (19). Then the  $q$ -HMC satisfies the detailed balance principle, i.e.,*

$$\pi(z)P(z \rightarrow z') = \pi(z')P(z' \rightarrow z).$$

*Proof.* By Proposition 1, it is easy to verify that  $\pi(z)\kappa(z \rightarrow z') = \frac{1}{J}\pi(z')\kappa(z' \rightarrow z)$ , where  $J = \det(\frac{\partial \Psi}{\partial z})_q$ . Therefore we have

$$\pi(z)\kappa(z \rightarrow z')\alpha(z \rightarrow z') = \frac{1}{J}\pi(z')\kappa(z' \rightarrow z)\alpha(z \rightarrow z').$$

By the definition of the accept probability  $\alpha$ , we know that

$$\pi(z)\kappa(z \rightarrow z')\alpha(z \rightarrow z') = \pi(z')\kappa(z' \rightarrow z)\alpha(z' \rightarrow z).$$

By this, we get the conclusion.  $\square$

We consider the common-used Hamiltonian  $H$

$$H(x, p) = U(x) + \frac{p^T M^{-1} p}{2}, \quad (22)$$

where  $M$  is a symmetric positive definite constant matrix. For this Hamiltonian, we can verify that the Hamiltonian system (11) is symplectic. And the Leap-Frog scheme preserves symplectic.

## 4 Numerical tests for potentials with analytical form

In the numerical tests, we compute the integrated autocorrelation time (IAT), which serves as the standard metric to quantify the mixing speed of the MCMC sampler. The IAT is defined as the number of sequential MCMC steps required to yield one effective, independent sample. The IAT is calculated from the sample's autocorrelation function ( $\rho_k$ ), which measures the linear dependence between samples separated by a lag  $k$ . The IAT ( $\tau$ ) is formally computed as

$$\tau = 1 + 2 \sum_{k=1}^{\infty} \rho_k, \quad (23)$$

where  $\rho_k$  is the autocorrelation at lag  $k$ . In practice, the summation is truncated at a finite lag  $k_{\max} = 500$  to ensure stability. A smaller IAT indicates faster mixing and higher efficiency. This IAT is then used to determine the effective sample size (ESS), defined as  $\text{ESS} = N/\tau$ , where  $N$  is the total number of samples collected. The overall sampler performance is reported as the ESS per unit of time (ESS/time), which serves as the final, absolute measure of efficiency. To compare the efficiency with  $q$ -HMC, we compute the derivative using the forward difference in the classical HMC in Example 2, 1, 3 and the exact one in Example 4, 5 respectively. The time step size  $\Delta t$  is fixed at 0.1 and the final time is taken as 1.

**Example 1** (Double well potential).

$$U(x) = (x^2 - 1)^2. \quad (24)$$

The initial state  $x$  is taken as 4. In Fig. 1, we show comparable accuracy for  $q = 0.95$  and  $q = 1.05$  of the sampling performance of  $q$ -HMC against classical HMC ( $q = 1$ ). The optimal sampling efficiency is achieved at a non-unity value of  $q$  ( $q = 1.02$ ), which is close to  $q = 1$ .

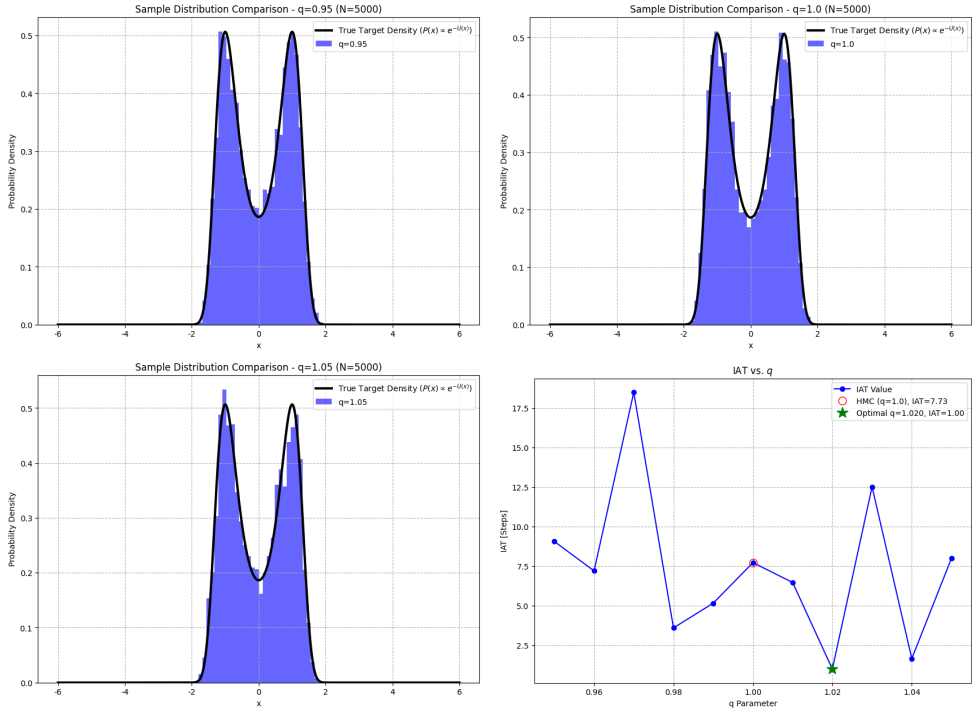


Figure 1: Sampling results for Example 1.

**Example 2** (Super-Flat Potential).

$$U(x) = |x|^{1/2}. \quad (25)$$

The initial state is set to  $x = 4$ . Numerical results are presented in Fig. 2. Chains for all  $q$  values exhibit substantial exploration of the parameter space (e.g., frequently crossing  $x = 0$ ). Their mixing efficiency is different for varying  $q$  values. The ACF for the optimal  $q$  decays faster than those for other  $q$  values, including standard HMC ( $q = 1$ ). This directly corresponds to a lower IAT, indicating that the optimal  $q$  achieves more statistically efficient sampling per iteration.

**Example 3** (Discontinuous potential).

$$U(x) = \begin{cases} 0.5x^2, & x < 0, \\ 0.5x^2 + 3, & x \geq 0. \end{cases} \quad (26)$$

The initial state is taken as  $x = 4$ . This result further underscores the flexibility of the  $q$ -HMC framework. As depicted in Fig. 3, the optimal value of the deformation

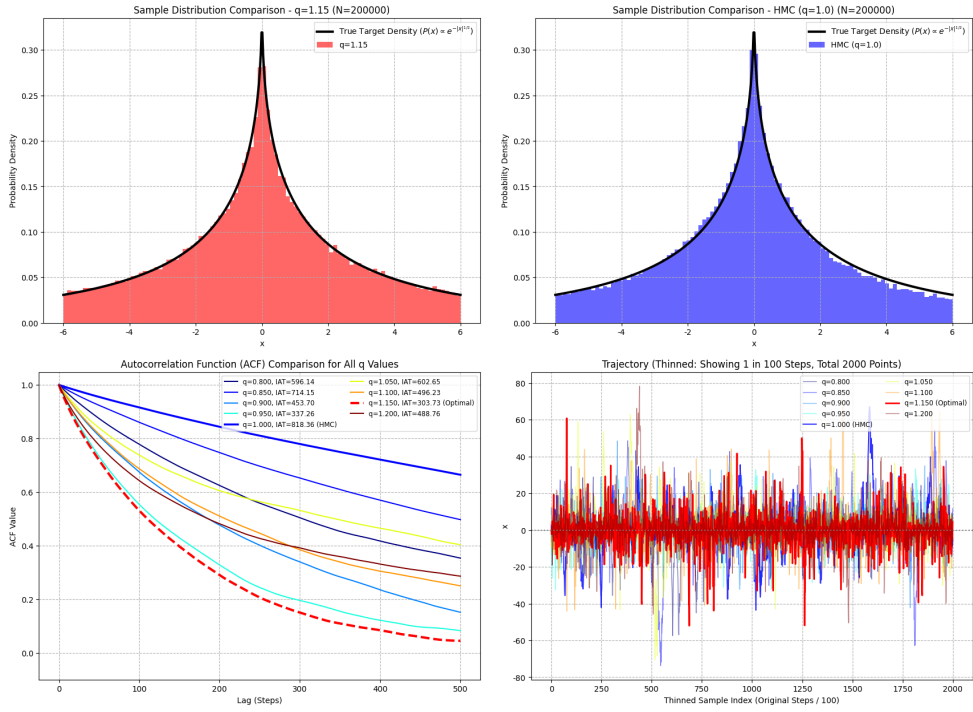


Figure 2: Sampling results for Example 2.

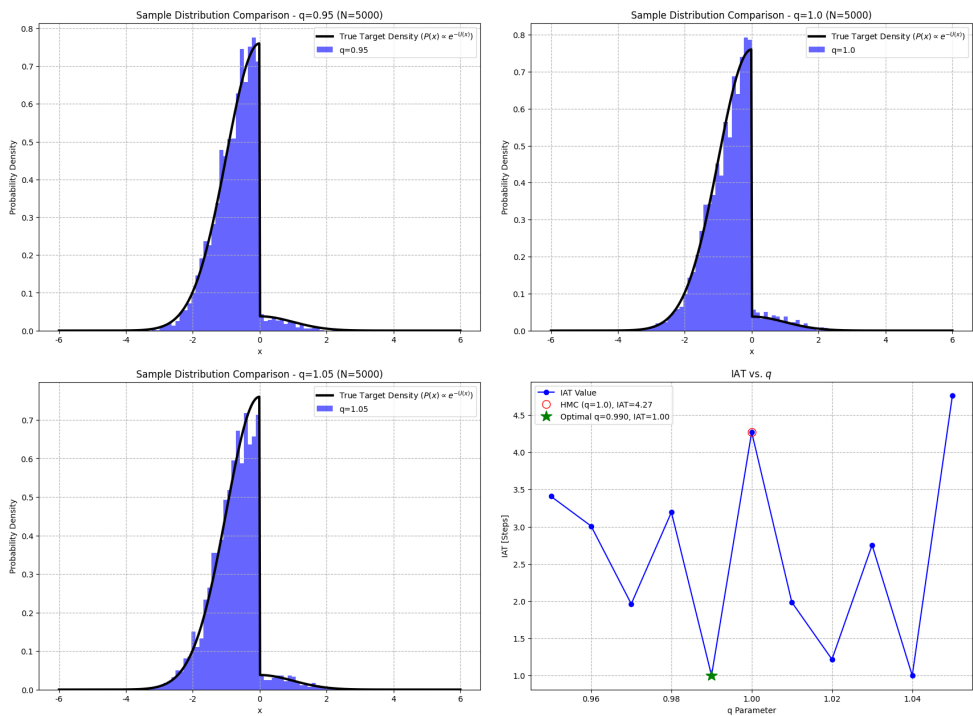


Figure 3: Sampling results for Example 3.

parameter lies near the classical limit at  $q_{\text{opt}} = 0.99$ . These results demonstrate that the  $q$ -HMC not only achieves efficiency comparable to classical HMC but also exhibits a notable capability in traversing a high potential energy barrier.

**Example 4** (Highly stiff potential).

$$U(x) = x^8 \quad (27)$$

The table below (see Table 1) shows the magnitude of the force ( $|F|$ ) acting on the particle at the initial position  $x = 1.7$ , which is a high-gradient point for the integrator.

Table 1: Force magnitudes for different  $q$  values at the high-gradient point.

$q$	Reference Point ( $q^2 x$ )	$\mathcal{D}_x U(x)$	Force Magnitude ( $ F $ )
1.0	N/A	328.06	328.06
0.9	1.377	170.81	161.76
1.1	2.057	468.61	491.54

Table 2: q-HMC Performance Metrics Across Various  $q$  Values.

$q$	Time (s)	Accept Rate	ESS	IAT (steps)	ESS/Time (Efficiency)
0.000	2.24	1.000	nan	N/A	nan
0.063	2.25	0.547	3927	2.55	1741.92
0.126	1.93	0.587	2035	4.91	1055.92
0.189	1.89	0.622	1968	5.08	1043.29
0.253	1.89	0.663	2247	4.45	1188.70
0.316	1.94	0.693	2148	4.66	1108.54
0.379	1.98	0.709	2030	4.93	1024.97
0.442	1.92	0.743	1909	5.24	996.26
0.505	1.90	0.755	1766	5.66	929.30
0.568	1.91	0.766	2691	3.72	1408.85
0.632	1.91	0.797	3732	2.68	1951.39
0.695	1.97	0.806	3395	2.95	1721.08
0.758	1.96	0.844	4049	2.47	2064.80
0.821	1.91	0.880	2710	3.69	1415.07
0.884	2.04	0.916	4027	2.48	1969.87
0.947	1.91	0.962	5252	1.90	2756.49 ( $\leftarrow$ BEST)
1.000	0.67	1.000	nan	N/A	nan
1.011	2.09	1.000	nan	N/A	nan
1.074	1.96	1.000	nan	N/A	nan
1.137	1.97	1.000	nan	N/A	nan
1.200	1.98	1.000	nan	N/A	nan

- 1. Classical Instability:** The classical HMC integrator is subject to a massive force of 328.06 at  $x = 1.7$ . When using a non-infinitesimal step size ( $\Delta t = 0.1$ ), this huge force rapidly introduces numerical error, causing the Hamiltonian ( $H$ ) to spike and leading to trajectory failure or near-certain rejection.

Table 3: 2D  $q$ -HMC Performance Metrics for  $U(x) = \frac{1}{8}(x_1^2 + x_2^2)^4$  (Analyzed on  $x_1$ ).

$q$	Time (s)	Accept Rate	ESS	IAT (steps)	ESS/Time (Efficiency)
0.000	5.00	1.000	nan	N/A	nan
0.058	4.45	0.421	1453	6.88	326.55
0.116	4.31	0.488	1058	9.45	245.81
0.174	4.33	0.521	3256	3.07	752.44
0.232	4.34	0.548	2882	3.47	663.94
0.289	4.26	0.576	10000	1.00	2348.83
0.347	4.38	0.603	3125	3.20	712.80
0.405	4.28	0.630	10000	1.00	2338.34
0.463	4.79	0.642	5615	1.78	1170.93
0.521	4.37	0.674	2327	4.30	532.86
0.579	4.33	0.711	4371	2.29	1009.58
0.637	4.52	0.739	10000	1.00	2211.45
0.695	4.77	0.773	10000	1.00	2096.63
0.753	4.23	0.805	10000	1.00	2362.90 ( $\leftarrow$ BEST)
0.811	4.59	1.000	nan	N/A	nan
0.868	4.31	1.000	nan	N/A	nan
0.926	4.33	1.000	nan	N/A	nan
0.984	4.39	1.000	nan	N/A	nan
1.000	3.96	1.000	nan	N/A	nan
1.042	4.24	1.000	nan	N/A	nan
1.100	4.21	1.000	nan	N/A	nan

2.  **$q$ -Force Reduction:** The  $q = 0.9$  generalized dynamics, which uses the Jackson  $q^2$ -derivative, calculates the force by referencing a "smoother" region of the potential at  $q^2 x = 1.377$  (a point closer to  $x = 0$ ).
3. **Numerical Robustness:** By effectively **reducing the magnitude of the acting force by 50.7%** in the initial, high-gradient step, the  $q$ -Leapfrog integrator prevents the particle's momentum from being excessively perturbed. This maintains the necessary approximate conservation of the Hamiltonian ( $H$ ), allowing the trajectory to complete and resulting in the high acceptance rates and superior efficiency observed in the simulation results.

We then evaluate the numerical performance for different values of  $q$  in Table 2. The sampling results for  $q = 0.9$  and  $q = 0.947$  are presented in Fig. 4. The results indicate that sampling fails for  $q \geq 1$  and  $q = 0$ , while high efficiency is achieved for values of  $q$  close to 1, suggesting an optimum near the classical limit.

**Example 5** (2-d highly stiff potential).

$$U(x_1, x_2) = \frac{1}{8}(x_1^2 + x_2^2)^4. \quad (28)$$

The 2d target distribution governed by the highly stiff potential presents a significant challenge for classical sampling methods, including standard HMC ( $q = 1.0$ ). The initial state was set to a high potential region at  $(x_1, x_2) = (1.6, 1.6)$ .

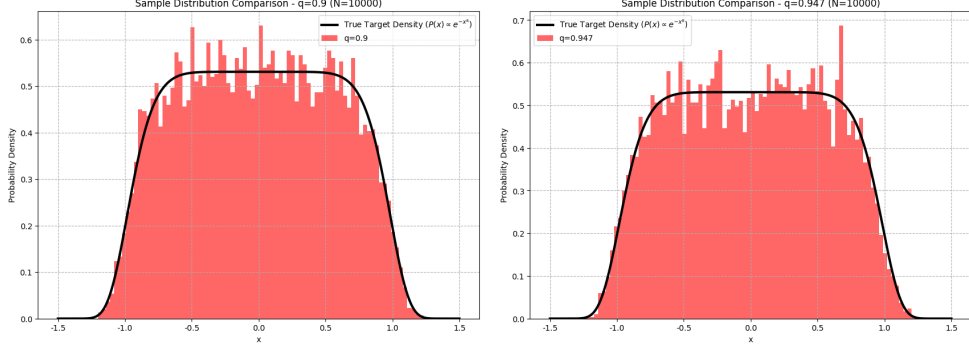


Figure 4: Sampling results for Example 4.

As detailed in Table 3, the performance of the classic HMC ( $q = 1.0$ ) is severely degraded, resulting in poor statistical estimates (indicated by  $\text{ESS} = \text{nan}$ ). However, the  $q$ -HMC method drastically improves mixing, achieving an optimal efficiency at  $q = 0.753$ . This optimal setting yields an ESS/Time efficiency of 2362.90 ESS/s, which is a dramatic improvement over the failed  $q = 1.0$  run.

The runs outside of this optimal range demonstrate the trade-off. Very low  $q$  values (e.g.,  $q = 0.000$ ) lead to  $q$ -dynamics that are too stiff or sticky, preventing the chain from effectively exploring the distribution and thus causing high rejection rates or completely stalling the chain, resulting in failure ( $\text{ESS} = \text{nan}$ ). Conversely, high  $q$  values (e.g.,  $q > 1.1$ ) create trajectories that are too volatile for the highly stiff  $U(x)$ . The resulting large  $\Delta H$  proposals lead to near-zero Metropolis acceptance probabilities, again causing the sampling run to fail.

The robustness of the optimal  $q$ -HMC is visually confirmed by the sample distribution in Fig. 5, which accurately reproduces the target distribution and exhibits efficient exploration of high-probability regions, as evidenced by its rapidly decaying ACFs.

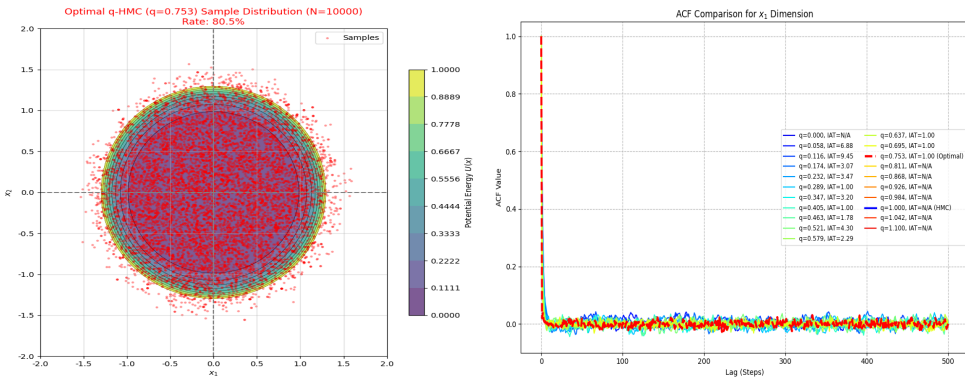


Figure 5: Sampling results for Example 5.

## 5 Application to Bayesian inverse problems

### 5.1 Gravity potential problem

**Example 6.** We first consider a simplified geophysics inverse problem aimed at estimating the depth  $h$  of a subsurface point mass based on gravity measurements taken at the surface. The gravitational anomaly  $g(h, x_s)$  measured by a sensor at a horizontal location  $x_s$  due to a point mass fixed at  $(x_f, h)$  is given by

$$g(h, x_s) = \frac{h}{((x_s - x_f) + h^2)^{3/2}}. \quad (29)$$

We set the true depth  $h = 0.2$ ,  $x_f = 0.3$  and collect the data at 5 sensors distributed uniformly at  $(0, 1)$ . The data is added the Gaussian noise with mean variance 0.1, i.e.,

$$\mathbf{d}_j = g(0.2, x_s(j)) + \mathcal{N}(0, \sigma^2), \quad j = 1, 2, \dots, 5, \quad (30)$$

where  $x_s = \{0, 0.25, 0.5, 0.75, 1\}$ ,  $\sigma = 0.1$ .

In Bayesian framework, the posterior distribution potential is

$$U_{\text{post}} = \frac{1}{2\sigma^2} \sum_{j=1}^5 |g(h, x_s(j)) - \mathbf{d}_j|^2 - \log \pi_0(h), \quad (31)$$

where  $\pi_0(h)$  is the prior density for  $h$ . Here we take  $\pi_0(h) = \mathcal{N}(0.3, 0.05^2)$ . In HMC, the derivative is computed using the forward difference with step size  $1e-8$ , which provides sufficient approximation for the derivative. To compare, we take  $q = 0.9999$  in  $q$ -HMC. The time step size  $\Delta t = 0.00025$  and  $L = 800$ . We generate 2,000 samples and the accept rate is 0.979 for  $q = 0.9999$  and 0.933 for  $q = 1$ . The numerical results are displayed in Fig. 6. The estimated probability is obtained by the accepted samples after 200 burn-in steps. From the displayed results, we can see that the  $q$ -HMC gives a better reconstruction than HMC.

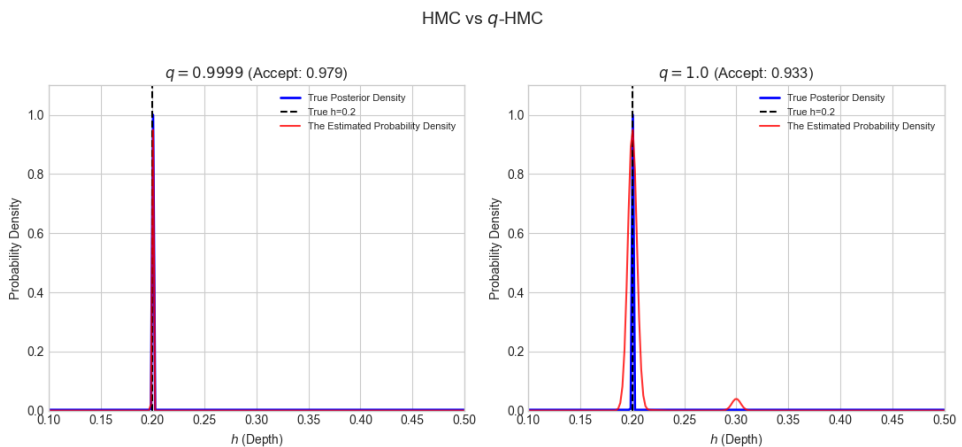


Figure 6: Sampling results for gravity potential problem in Example 6.

## 5.2 An infinite-dimensional inverse problem

We consider inverse problems with functional parameter occurring in partial differential equations. The state variable  $u$  and the system parameter of interest  $\alpha$  are governed by the system

$$\mathcal{F}(u; \alpha) = 0, \quad (32)$$

that satisfies the prescribed initial and boundary value conditions. We aim to minimize the functional

$$\mathcal{J}(\alpha) = \frac{1}{2} \sum_j |u(x_j; \alpha) - \mathbf{d}_j|^2, \quad (33)$$

where  $x_j$ 's are the measure locations,  $\mathbf{d}_j = u(x_j; \alpha) + \xi$  is the measured data at  $x_j$  with  $\xi \sim \mathcal{N}(0, \sigma^2)$  and  $u$  is the solution to (32) with parameter  $\alpha$ . Within the Bayesian inversion framework,  $\exp(-\frac{1}{\sigma^2} \mathcal{J})$  represents the likelihood function. Assigning a prior distribution  $\pi_0$  to the unknown parameter  $\alpha$  leads, via Bayes's formula, to the posterior

$$\pi(\alpha) \propto \exp\left(-\frac{1}{\sigma^2} \mathcal{J}(\alpha)\right) \pi_0(\alpha). \quad (34)$$

We subsequently investigate the distribution using the  $q$ -HMC framework.

For fixed  $y \in \Omega$ , define the perturbed field

$$\alpha_{q,y}(x) = \begin{cases} \alpha(x), & x \neq y, \\ q^2 \alpha(y), & x = y. \end{cases} \quad (35)$$

The corresponding state is denoted by  $u_{q,y}$ . The  $q$ -Jackson derivative is then given by

$$\mathcal{D}_{\alpha(y)} \mathcal{J}(\alpha) := \frac{\mathcal{J}(\alpha_{q,y}) - \mathcal{J}(\alpha)}{(q^2 - 1)\alpha(y)}. \quad (36)$$

Denoting  $\delta u_{q,y} := u_{q,y} - u$ , we have

$$\mathcal{J}(\alpha_{q,y}) - \mathcal{J}(\alpha) = \sum_j (u(x_j; \alpha) - \mathbf{d}_j) \delta u_{q,y}(x_j) + O(|\delta u|^2). \quad (37)$$

We omit the second order term and get the first order approximation

$$\mathcal{J}(\alpha_{q,y}) - \mathcal{J}(\alpha) \approx \sum_j (u(x_j) - \mathbf{d}_j) \delta u_{q,y}(x_j). \quad (38)$$

The linearization of  $\mathcal{F}$  at  $(u, \alpha)$  gives

$$\mathcal{F}(u_{q,y}; \alpha_{q,y}) \approx \mathcal{F}(u; \alpha) + \frac{\partial \mathcal{F}}{\partial u} \delta u_{q,y} + \frac{\partial \mathcal{F}}{\partial \alpha} \delta \alpha_{q,y} = 0, \quad (39)$$

where  $\delta \alpha_{q,y}(x) = (q^2 - 1)\alpha(y)\delta(x - y)$ . It follows that

$$\frac{\partial \mathcal{F}}{\partial u} \delta u_{q,y} = -\frac{\partial \mathcal{F}}{\partial \alpha} [(q^2 - 1)\alpha(y)\delta(x - y)], \quad (40)$$

i.e.,

$$L\delta u_{q,y} = -(q^2 - 1)\alpha(y)A_y, \quad (41)$$

whereas  $L = \frac{\partial \mathcal{F}}{\partial u}$  and  $A_y = \frac{\partial \mathcal{F}}{\partial \alpha}\delta_y$ . The adjoint operator of  $L$  satisfies

$$L^*\lambda = \sum_j (u(x_j) - \mathbf{d}_j)\delta(x - x_j), \quad (42)$$

where  $\lambda$  is the adjoint variable. We hence get that

$$\sum_j (u(x_j) - \mathbf{d}_j)\delta u_{q,y}(x_j) = \langle L^*\lambda, \delta u_{q,y} \rangle = \langle \lambda, L\delta u_{q,y} \rangle. \quad (43)$$

Inserting (41) into (43), we have

$$\sum_j (u(x_j) - \mathbf{d}_j)\delta u_{q,y}(x_j) = -(q^2 - 1)\alpha(y)\langle \lambda, A_y \rangle. \quad (44)$$

In addition, we have

$$\langle \lambda, A_y \rangle = \langle \lambda, \frac{\partial \mathcal{F}}{\partial \alpha}\delta_y \rangle = [(\frac{\partial \mathcal{F}}{\partial \alpha})^*\lambda](y) := G(y). \quad (45)$$

This yields that

$$\sum_j (u(x_j) - \mathbf{d}_j)\delta u_{q,y}(x_j) = -(q^2 - 1)\alpha(y)G(y). \quad (46)$$

This shows that

$$\mathcal{D}_{\alpha(y)}\mathcal{J}(\alpha) = -G(y) = -[(\frac{\partial \mathcal{F}}{\partial \alpha})^*\lambda](y). \quad (47)$$

**Remark 1.** Formulation (47) shows that the  $q$ -HMC is equivalent to the classical case in computation when dealing with the inverse problems.

**Example 7.**

$$\begin{cases} -\nabla \cdot (\alpha(x)\nabla u) = f(x), & x \in \Omega, \\ u(x) = 0, & x \in \partial\Omega. \end{cases} \quad (48)$$

The data is collected on some scattered points  $\{x_i\} \in \Omega$ ,  $i = 1, 2, \dots, M$ . We reconstruct the diffusion coefficient  $\alpha$  according to the noisy data  $\mathbf{d}_i = u(x_i; \alpha) + \eta_i$  with  $\eta_i \sim N(0, \sigma^2)$ . The forward problem is denoted by

$$\mathcal{G}(\alpha) = \mathbf{d}. \quad (49)$$

In this example, the  $q$ -Jackson derivative of the functional  $\mathcal{J}$  is

$$\mathcal{D}_{\alpha(y)}\mathcal{J}(\alpha) = -\left[ (\frac{\partial \mathcal{F}}{\partial \alpha})^*\lambda \right](y) = -\nabla u(y) \cdot \nabla \lambda(y), \quad (50)$$

where this adjoint variable  $\lambda$  satisfies

$$\begin{cases} -\nabla \cdot (\alpha \nabla \lambda) = \frac{1}{\sigma^2} \sum_{i=1}^M (u(x_i) - \mathbf{d}_i) \delta(x - x_i), & x \in \Omega, \\ \lambda(x) = 0, & x \in \partial\Omega. \end{cases} \quad (51)$$

The potential function is given by

$$U(\alpha) = \frac{1}{\sigma^2} \mathcal{J}(\alpha) - \log \pi_0(\alpha). \quad (52)$$

The kinetic energy function is defined as  $K(p) = \frac{p^T M^{-1} p}{2}$ , and thus the total energy is

$$H(\alpha, p) = U(\alpha) + K(p). \quad (53)$$

The inverse diffusion problem is considered on the 1-dimensional domain  $\Omega = [0, 1] \in \mathbb{R}$ . The true diffusion coefficient is taken as  $\alpha(x) = \exp(0.15 \sin(2\pi x) + 0.05 \sin(4\pi x))$ .

We parameterize the diffusion coefficient  $\alpha(x) = \exp(\kappa(x))$ , where the log-permeability  $\kappa$  is assumed to be a Gaussian process  $\kappa \sim N(0, \Gamma)$ . The covariance operator  $\Gamma$  is related to negative Laplace operator, specifically  $\Gamma = (-\Delta)^{-s}$  with  $s > 0$  subject to some boundary condition, which enforces spatial smoothness. The Karhunen-Loëve (KL) expansion of  $\kappa$  is

$$\kappa(x) = \sum_{k=1}^{\infty} \mu_k \varphi_k(x), \quad (54)$$

where  $\{\mu_k; \varphi_k\}$  is the eigensystem of the covariance operator  $\Gamma$ .

The spatial domain is discretized into  $N = 80$  finite difference grid points. To ensure computational tractability, we retained the  $K = 9$  most significant KL modes for the sampling procedure, resulting in a low-dimensional sampling space. The system is constrained by  $M = 70$  noisy observations corrupted by Gaussian noise with a standard deviation of  $\sigma = 0.02$  (Fig. 7: Right).

The parameter space is explored using the  $q$ -HMC sampler. The sampler is executed for 100,000 iterations with 20 leapfrog steps per trajectory. An adaptive step-size mechanism was implemented during the initial 20,000 steps, targeting an optimal acceptance rate of 50%. The initial step size  $\Delta t = 0.15$  and it is successfully tuned to a final, stable value of  $\Delta t \approx 0.224$ . The overall acceptance rate achieved is 62.4%. While this rate is slightly higher than the commonly recommended range of 60%-70%, it confirms that the sampler efficiently proposes distant states with a high probability of acceptance, indicative of good mixing. The potential energy trace (Fig. 7: Middle) shows quick convergence, stabilizing around an expected minimum energy level shortly after the burn-in period. The posterior mean of the parameter field  $\alpha(x)$  was calculated using the samples collected after a burn-in period of 10,000 steps. The reconstruction quality was assessed against the true parameter field (Fig. 7: Left). The reconstruction root mean square error (RMSE) is 0.0431, which demonstrates the accuracy of the posterior mean in fitting the observations while respecting the prior constraints. Furthermore, the correlation coefficient between the posterior mean and the truth is 0.9368. The state reconstruction is consistent with the true state (Fig. 7: Right). These results validate the strong numerical performance and parameter identification capability of the  $q$ -HMC method.

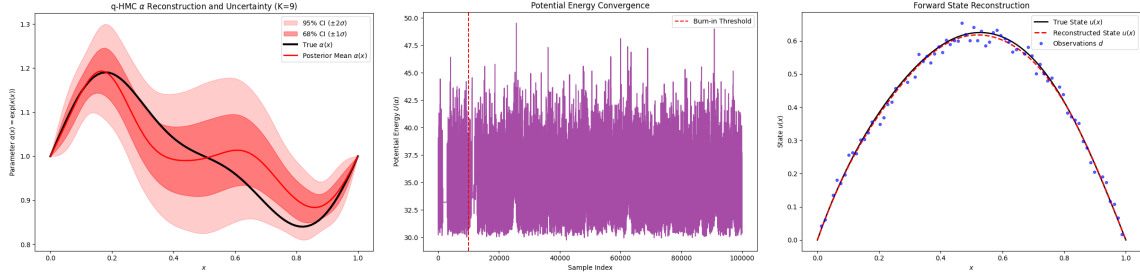


Figure 7: Reconstruction results.

## 6 Conclusions

We establish  $q$ -deformed Hamiltonian dynamics from Lagrange mechanics, leading to a tractable  $q$ -analog of classical Hamiltonian equations. A corresponding  $q$ -Hamiltonian Monte Carlo (q-HMC) algorithm is then constructed via Leap-Frog discretization. The method proves effective for general sampling tasks, particularly for distributions with stiff potentials, and is also applied to Bayesian inverse problems. Numerical experiments demonstrate its feasibility and effectiveness.

## References

- [1] V. Bardek and S. Meljanac. Deformed heisenberg algebras, a fock-space representation and the calogero model. *The European Physical Journal C*, 17(3):539–547, 2000.
- [2] M. Betancourt, S. Byrne, S. Livingstone, and M. Girolami. The geometric foundations of hamiltonian monte carlo. *Bernoulli*, 23(4A):2257–2298, 2017.
- [3] C. M. Bishop. *Pattern Recognition and Machine Learning*. Information Science and Statistics. Springer, New York, 2006.
- [4] N. Bou-Rabee, A. Eberle, and R. Zimmer. Coupling and convergence for hamiltonian monte carlo. *The Annals of Applied Probability*, 30(3):1209–1250, 2020.
- [5] B. L. Cerchiai, R. Hinterding, J. Madore, and J. Wess. A calculus based on a  $q$ -deformed heisenberg algebra. *The European Physical Journal C*, 8(3):547–558, 1999.
- [6] S. Duane, A. D. Kennedy, B. J. Pendleton, and D. Roweth. Hybrid monte carlo. *Physics Letters B*, 195:216–222, 1987.
- [7] A. Durmus, É. Moulines, and E. Saksman. Irreducibility and geometric ergodicity of hamiltonian monte carlo. *The Annals of Statistics*, 48(6):3545–3564, 2020.
- [8] R. J. Finkelstein. The  $q$ -coulomb problem. *Journal of Mathematical Physics*, 37(6):2628–2636, 1996.
- [9] R. J. Finkelstein.  $q$ -deformation of the lorentz group. *Journal of Mathematical Physics*, 37(2):953–964, 1996.

- [10] J. Gora. Two models of a  $q$ -deformed hydrogen atom. *J. Phys. A: Math. Gen.*, 25:L1281–L1285, 1992.
- [11] R. Hinterding and J. Wess.  $q$ -deformed hermite polynomials in  $q$ -quantum mechanics. *The European Physical Journal C*, 6(1):183–186, 1999.
- [12] S. Iida and H. Kuratsuji. Quantum algebra near  $q = 1$  and a deformed symplectic structure. *Phys. Rev. Lett.*, 69(13):1833–1836, 1992.
- [13] JMLR: W&CP. *Exponential integration for Hamiltonian Monte Carlo*, volume 37, Lille, France, 2015. Proceedings of the 32<sup>nd</sup> International Conference on Machine Learning.
- [14] M. Kibler and T. Négadi. On the  $q$ -analogue of the hydrogen atom. *J. Phys. A: Math. Gen.*, 24(22):5283–5289, 1991.
- [15] A. Lavagno. Basic-deformed quantum mechanics. *Reports on Mathematical Physics*, 64(1/2):79–91, 2009.
- [16] A. Lavagno and G. Gervino. Quantum mechanics in  $q$ -deformed calculus. In *Journal of Physics: Conference Series*, volume 174, page 012071. Fourth International Workshop DICE2008, 2009.
- [17] A. Lavagno, A.M. Scarfone, and P. Narayana Swamy. Classical and quantum  $q$ -deformed physical systems. *The European Physical Journal C*, 47:253–261, 2006.
- [18] S. Livingstone, M. Betancourt, S. Byrne, and M. Girolami. On the geometric ergodicity of hamiltonian monte carlo. *Bernoulli*, 25(4A):3109–3138, 2019.
- [19] D. J. C. MacKay. *Information Theory, Inference and Learning Algorithms*. Cambridge University Press, New York, 2003.
- [20] M. Micu. A  $q$ -deformed schrödinger equation. *J. Phys. A: Math. Gen.*, 32:7765–7777, 1999.
- [21] R. M. Neal. *Bayesian Learning for Neural Networks*. PhD thesis, University of Toronto, 1995.
- [22] R. M. Neal. *MCMC Using Hamiltonian Dynamics*. Handbook of Markov Chain Monte Carlo. CRC Press, New York., s. brooks, a. gelman, g. l. jones and x.-l. meng, eds. edition, 2011.
- [23] X. C. Song and L. Liao. The quantum schrödinger equation and the  $q$ -deformation of the hydrogen atom. *J. Phys. A: Math. Gen.*, 25:623–634, 1992.
- [24] M. R Ubriaco. Non-commutative differential calculus and q-analysis. *J. Phys. A: Math. Gen.*, 25:169–173, 1992.
- [25] J. Wess and B. Zumino. Covariant differential calculus on the quantum hyperplane. *Nuclear Physics B (Proc. Suppl.)*, 18B:302–312, 1990.
- [26] J. Z. Zhang. Perturbative equivalent theorem in  $q$ -deformed dynamics. *Physics Letters B*, 517:210–214, 2001.

[27] J. Z. Zhang and P. Osland. Perturbative aspects of  $q$ -deformed dynamics. *Eur. Phys. J. C*, 20(2):393–396, 2001.